Biomedical Measurement using NIR-light

seminar＠Hase

2012/06/28

NIR-wave

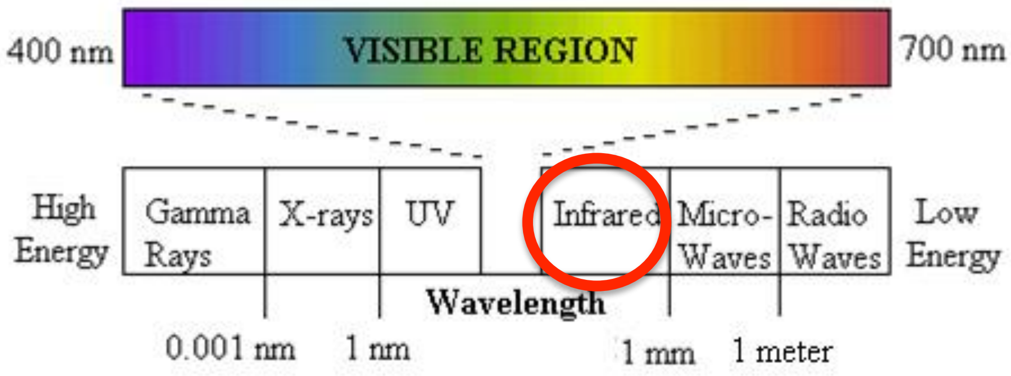

The Electromagnetic Spectrum

Biomedical Measurement

- Good penetration
- Low invasive
- Small size, low price (equipment)

problem

attenuation

Rayleigh scattering　　Absorption

Signal Intensity is proportional to λ^{-4}

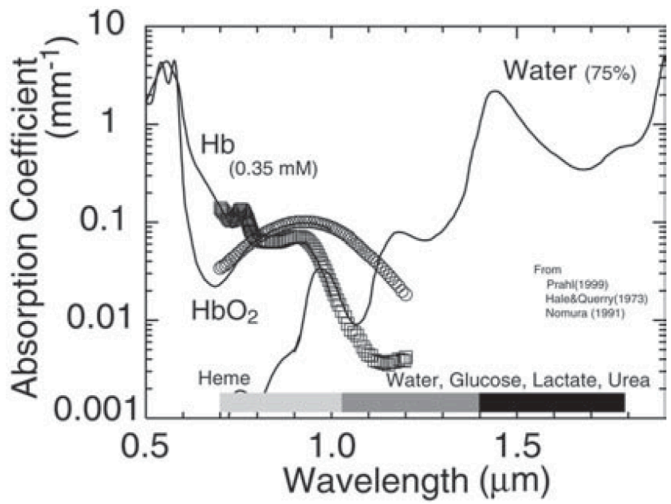

1. Quantitative comparison of contrast and imaging depth of ultrahigh-resolution optical coherence tomography images in 800–1700 nm wavelength region. Shutaro Ishida, Norihiko Nishizawa. BIOMEDICAL OPTICS EXPRESS 282 3 No.2 (2012)

2. Dentin micro-architecture using harmonic generation microscopy. R. Elbaum, E. Tal, A.I. Perets, D. Oron, D. Ziskind, Y. Silberberg, H.D. Wagner. journal of dentistry 35 150 – 155 (2007)

3. Multiphoton Microscopy of Ex Vivo Corneas after Collagen Cross-Linking. Juan M. Bueno,Emilio J. Gualda,Anastasia Giakoumaki,Pablo Pe´rez-Merino,Susana Marcos,and Pablo Artal. Investigative Ophthalmology & Visual Science 52 No. 8 (2011)

TD-OCT (time-domain optical coherence tomography)

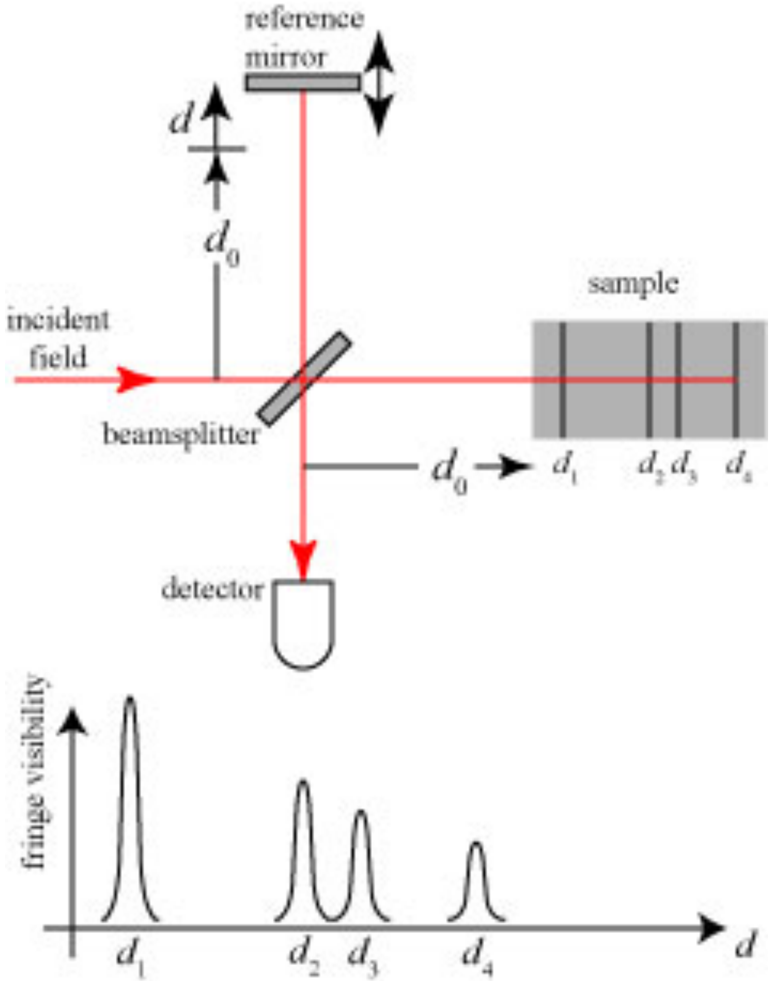

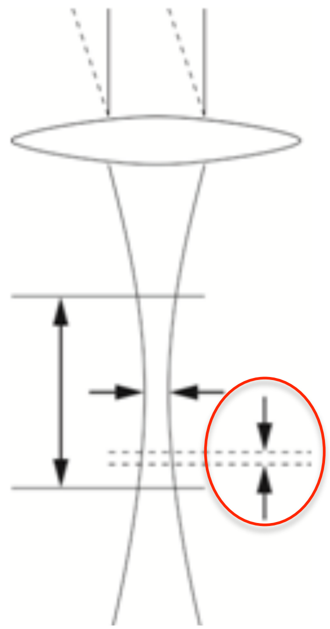

axial resolution

$$\delta z = l_c = \frac{2\ln 2}{\pi}\frac{\lambda_0^2}{\Delta\lambda}$$

OCT ➡ distribution of reflect signal intensity

Setup

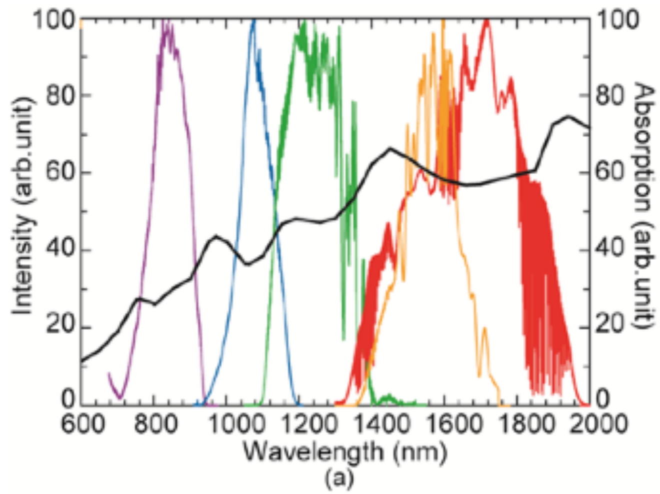

- supercontinuum sources at five wavelengths

800 nm - Ti:sapphire laser (Spectra Physics Mai-Tai HP)
1060 nm - Nd:glass laser (High Q Laser Production)
1300 nm - Er-doped fiber laser (IMRA femtolite B-5)
1550 nm - Er-doped fiber laser (custom-made)
1700 nm - Er-doped fiber laser (IMRA femtolite B-5)

- SC spectra fit in the valleys or flat regions of the water absorption spectrum (except for 1550nm)

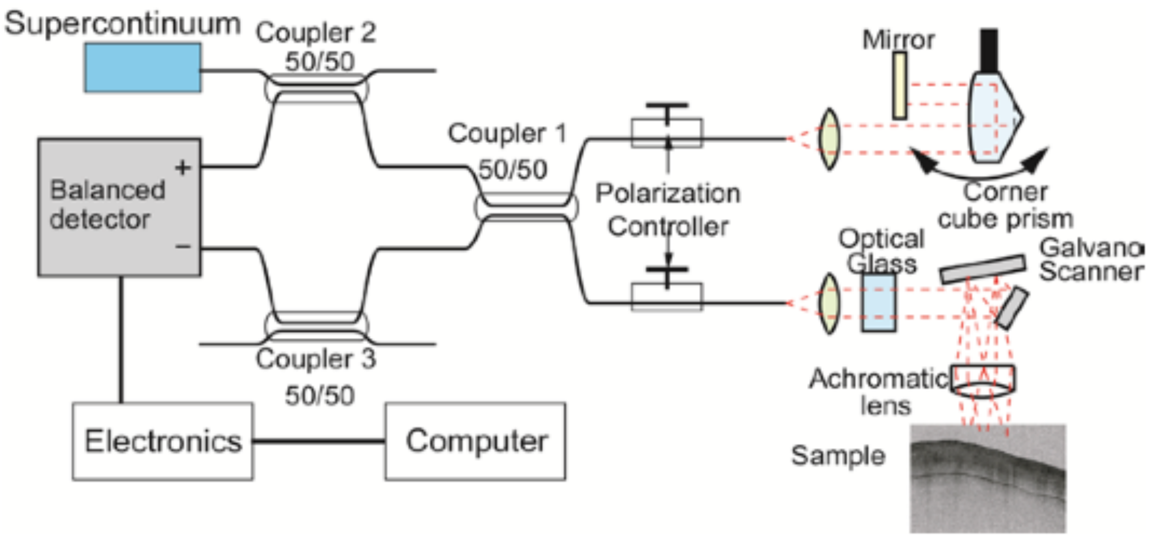

Result (1) : memory card

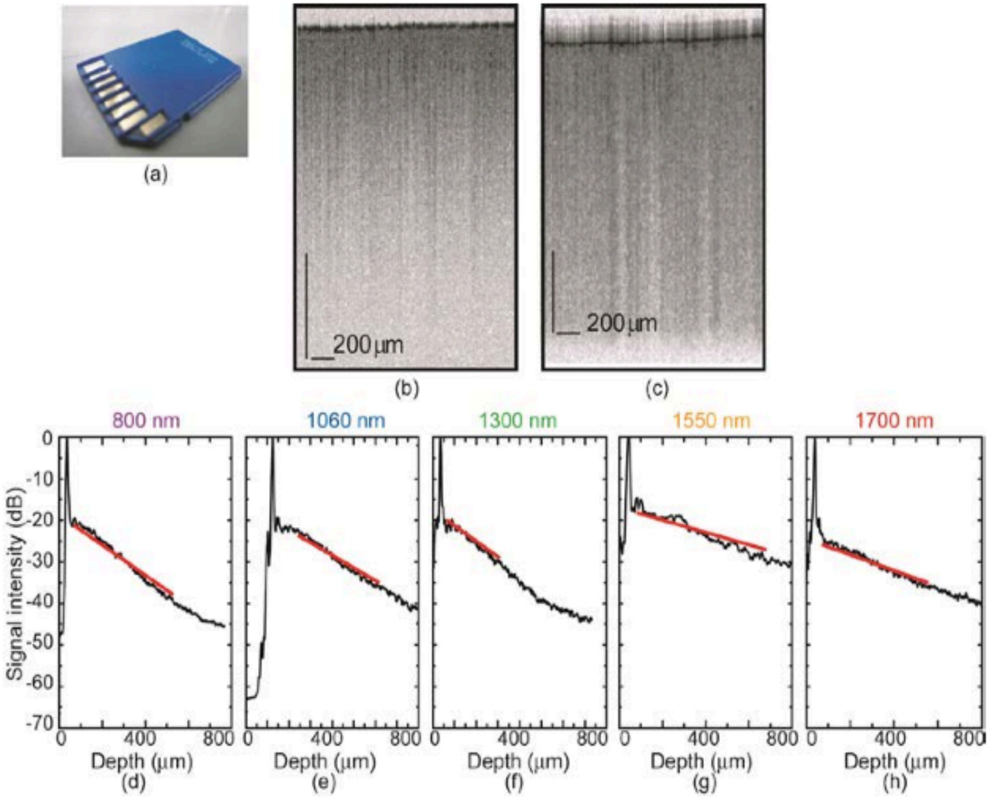

Longer wavelength

Lower slope

industrially used materials

↓

depend on scattering

Rayleigh scattering theory

Result (2) : pig trachea

The solid red line shows the slope at the mucosa layer.

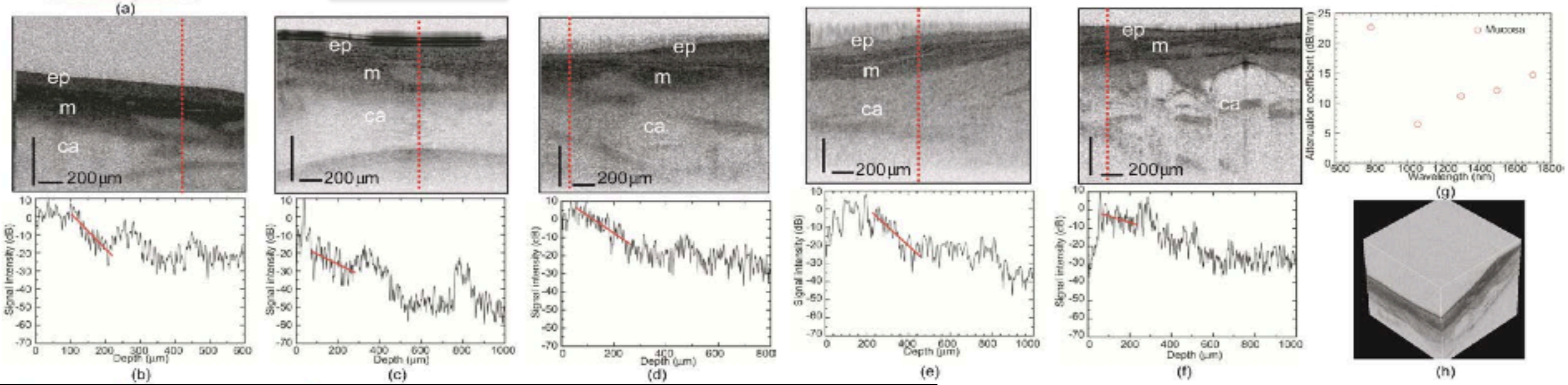

pig trachea → depend on absorption and scattering

The total attenuation coefficient is highest at 800 nm. → absorption by hemoglobin

At longer wavelengths, the total attenuation coefficient increased. → absorption by water

The image contrast was much clearer at 1700 nm than at the other wavelengths.

Result (3) : Total attenuation coefficients

industrially used materials

attenuation

scattering

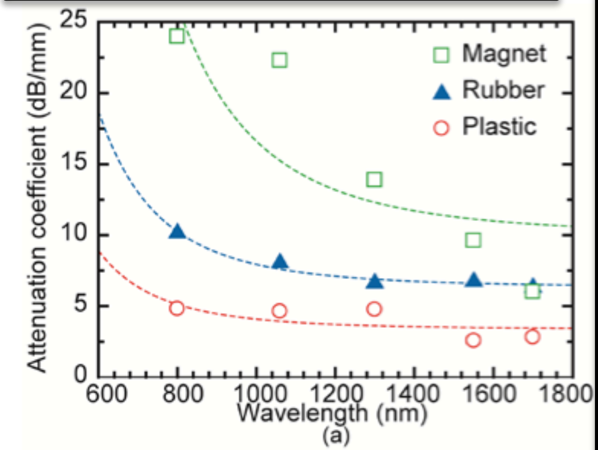

biomedical samples

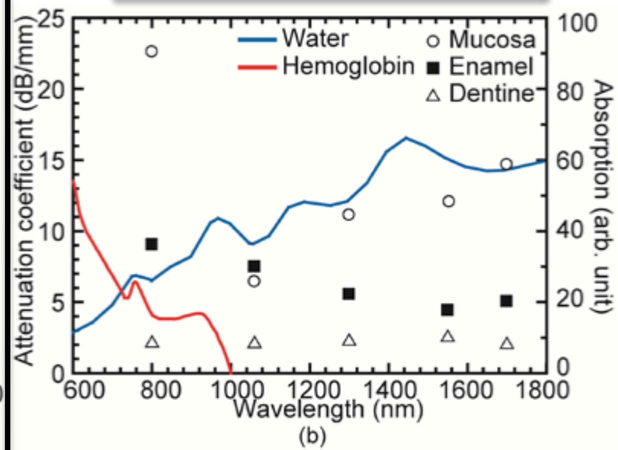

attenuation

absorption and scattering

- The total attenuation were well-fitted to the λ^{-4} dependence
- The longer-wavelength system is useful

- The enamel and dentine layers
  →same characteristics as the industrial samples
  →low absorption by water in human teeth
- The mucosa layer
  → dependent on the sum of absorption and scattering
- There is a trade-off between imaging contrast and total attenuation coefficient

Summary

- TD-OCT using supercontinuum sources at five wavelengths
  - 800 nm
  - 1060 nm
  - 1300 nm
  - 1550 nm
  - 1700 nm

- There have been no studies comparing the performance of ultrahighresolution optical coherence tomography (UHR-OCT) for the same sample over a wide wavelength range

This author investigated the wavelength dependence of the images for several different samples and quantitatively compared their optical properties.

Tooth & dentin

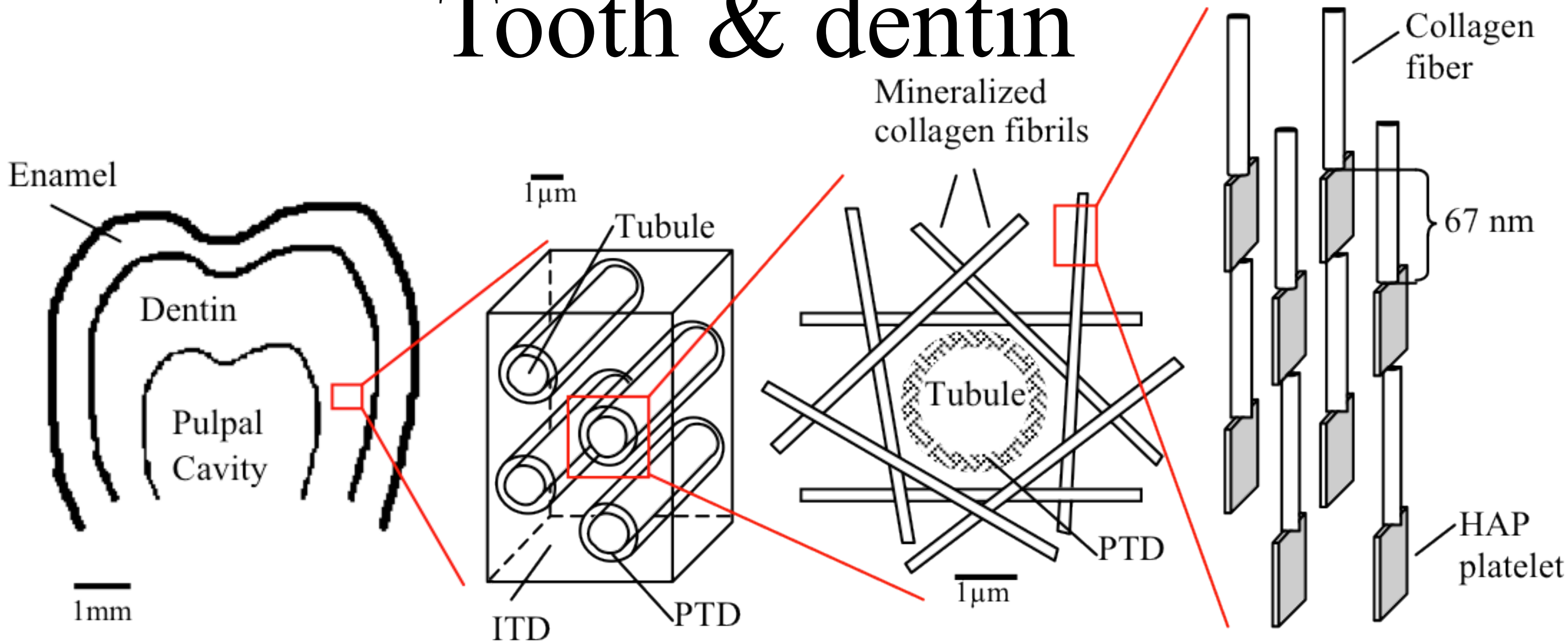

Dentin
- (dentinal) Tubule
- Peritubular dentin (PTD)
- intertubular dentin(ITD)

- Tubule is filled with the odontoblast cytoplasmatic fluid
- PTD → 10% by volume of collagen, mineralized thin cylinder
- ITD contains about 30 volume percent mineralized collagen Type I fibrils, wrapped around perpendicularly to the tubule long axis.

Setup of HGM

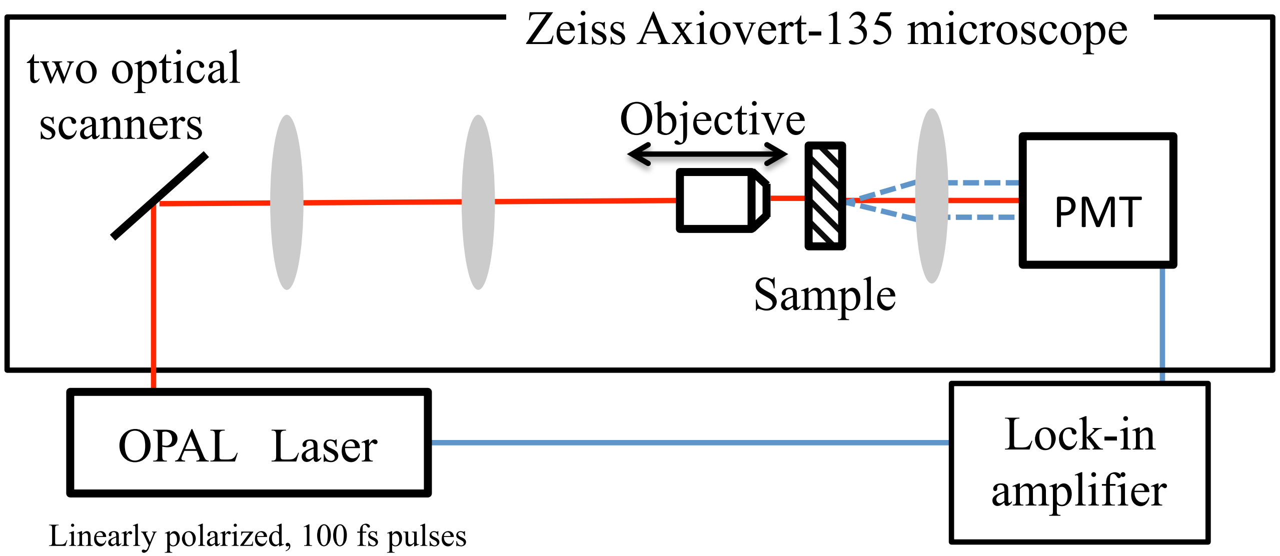

Linearly polarized, 100 fs pulses
wavelength of 1.5 μm
Repetition rate of 80 MHz

sample

Thin sections of about 200 μm

Each sections were sonicated for 45 min in solution before HGM measurement.

Table 1 – A lower anterior bovine incisor

Slice (immersion solution)	Approximate observation points	Density (tubules/mm^2)	Angle (°)
A (HBSS)	Deep dentin (1)	22,440	1
B (Murray)	Deep dentin (1)	20,550	21
	Deep dentin (2)	26,110	7
	Deep dentin (3)	24,440	10
	Deep dentin (4)	28,330	4
C (Murray)	Deep dentin (5)	40,550	1
	Shallow dentin (6)	n/a[a]	~90[a]
D (Murray)	Shallow dentin (6)	15,000	11

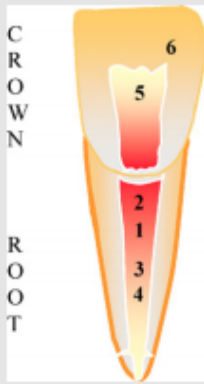

Various locations of the 3D HGM observation points are indicated on the illustration. The results of the 3D reconstruction present tubule density and orientation (angle). Slices A, B and C were facing the pulpal wall (deep dentin in the center, shallow dentin at the periphery) at various root locations. Tubules cut crosswise at different angles. Slice D was cut from the proximal side near the DEJ.

[a] Tubule orientation was almost parallel to the surface, thus no 3D reconstruction was possible; the angle was estimated.

THG(third harmonic generation)

$$P = P_L + P_{NL} = \varepsilon_0 \chi^{(1)} E + \varepsilon_0 \chi^{(2)} EE + \varepsilon_0 \chi^{(3)} EEE + \cdots$$

$$E = E_0 \sin \omega t \longrightarrow E^3 = \frac{1}{4} E_0^{\ 3} \left(3 \sin \omega t - \sin 3\omega t \right) \longrightarrow \text{THG}$$

reversed ***E*** in non-centrosymmetric materials ⟶ reversed ***P***

$$P_3 = \varepsilon_0 \chi^{(3)} EEE \qquad -P_3 = \varepsilon_0 \chi^{(3)} (-E)(-E)(-E)$$

THG signal is generated by every material.

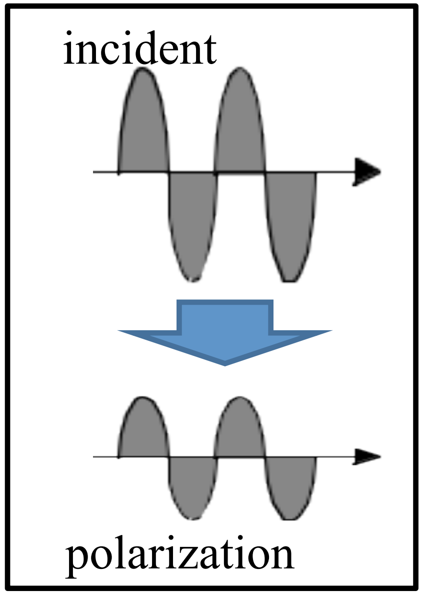

THG(third harmonic generation)

- THG signal generated before the focus of the excitation beam destructively interferes with the signal generated behind the focal plane.

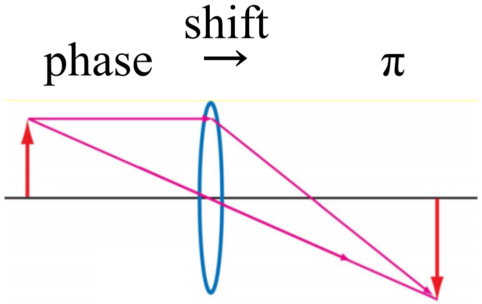

Guoy phase shift

phase shift @ before and after focal point

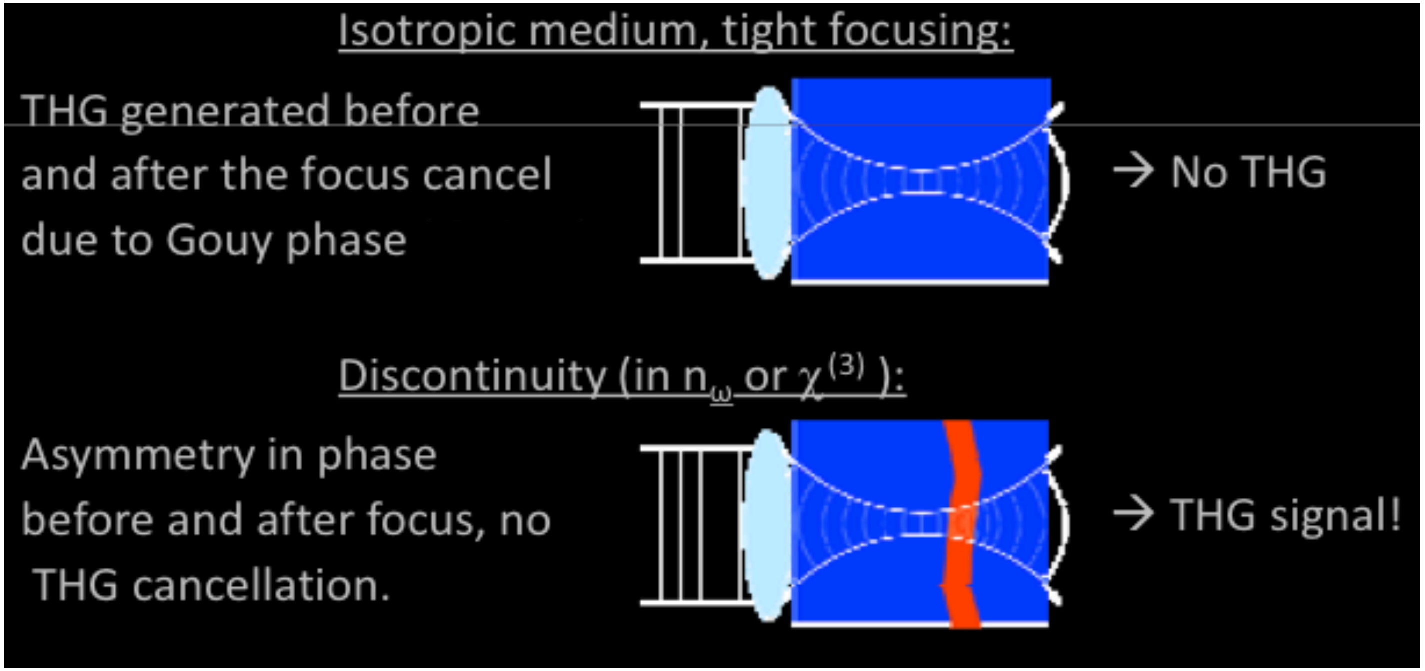

THG will be generated specifically at interfaces between materials of different third order nonlinear susceptibilities

Result (1) : THG, SHG, ESEM

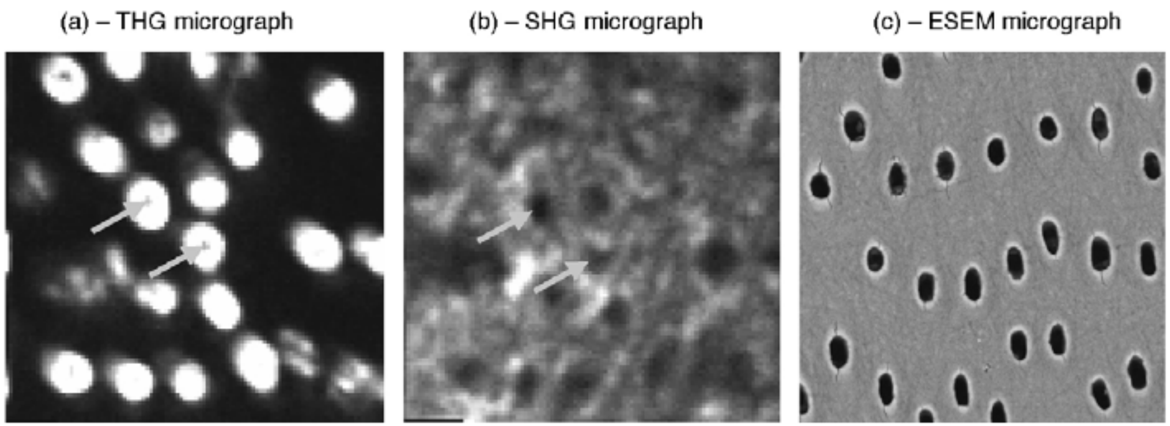

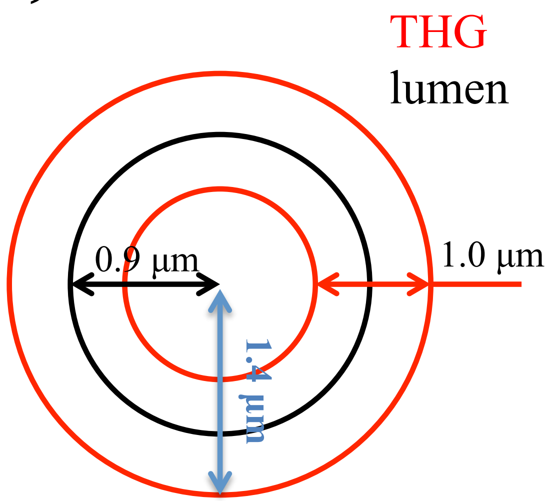

ESEM → variation in the mineralization level → tubules = black
PTD = white
ITD = gray

- The average radius of the lumen is about 0.9 μm.
- The spatial resolution of the THG image is about 1 μm.
- This means that a feature of about 0.9 mm in radius, like the lumen, will appear as ~1.5 μm in radius.
- The THG image displays bright circular features with an average radius of 1.54 μm.

➡ THG signal was created only at the lumen–PTD interface and not at the PTD–ITD interface

SHG → They contain much less collagen than the ITD
→ the tubules and the PTD appear in black

Result (2) :Overlays of SHG and THG images

Maximal SHG signal is obtained when the laser light polarization is parallel to the collagen fibrils.

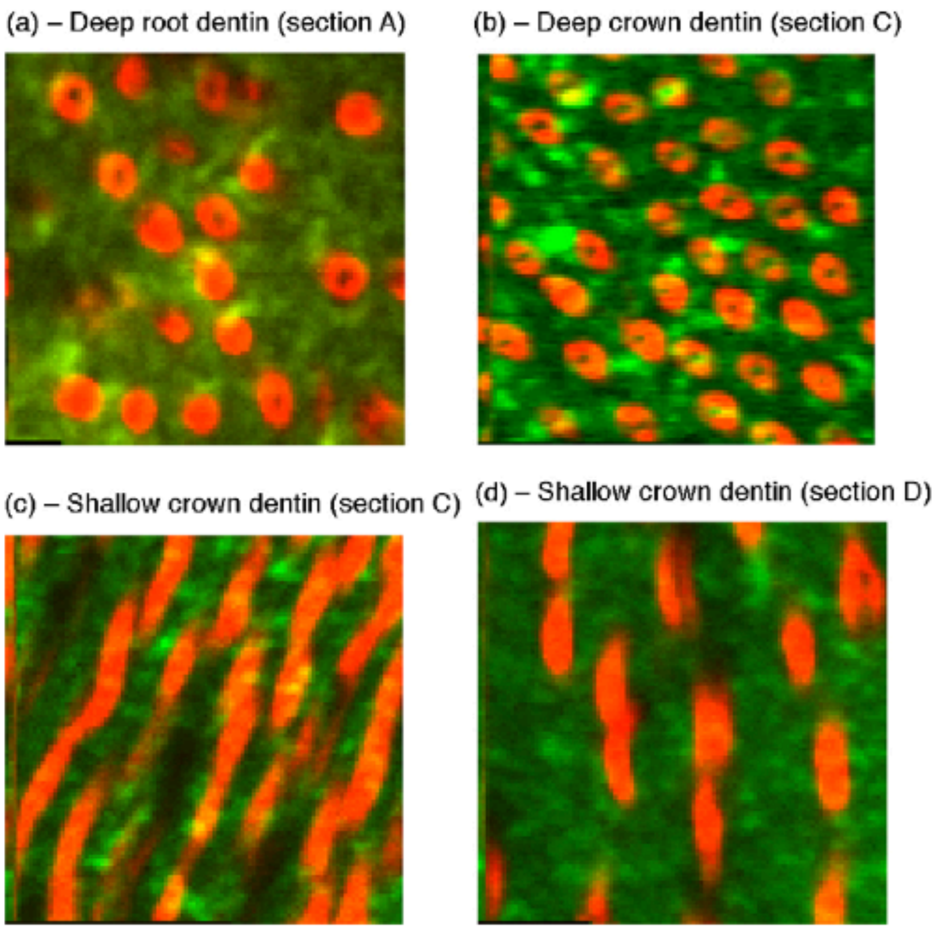

different region

- The direction of the tubules in relation to the sample surface was found to influence the image quality.

Tubules ⊥ sample surface

Strong SHG signal

(c) → dentin enamel junction (DEJ)

DEJ

Collagen fibrils lie parallel to the tubules long axis

Strong SHG signal

Result (3) :3D reconstruction

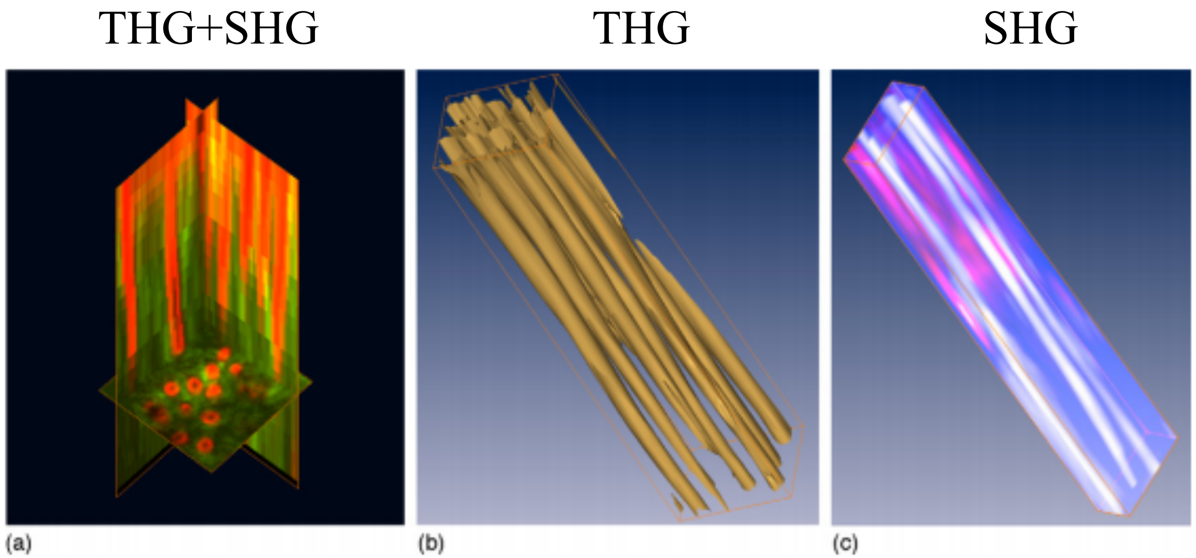

THG

- The tubules lie parallel to each other
- The tubules appear to narrow towards the bottom → loss of the signal at increased depths

SHG

High intensity signal = parallel to the tubules long axis

→ Such structures may be important with respect to the mechanical properties of the dentin

These structures could not be visualized in the 2D data.

Summary

- This work presents the micro-architecture of tooth dentin reconstructed from harmonic generation micrographs.

- The major advantage over other imaging methods is the ability to locate features within the dentin 3D space.

- The information includes two features: The tubule surfaces, observed using THG signal, and collagen, observed through SHG signal.

- This method may be incorporated in many topics related to the research on dentin, such as the hybridization of dentin with artificial materials, primary dentin development versus secondary dentin, dentin bacterial infection, and crack formation.

Cornea

Eye

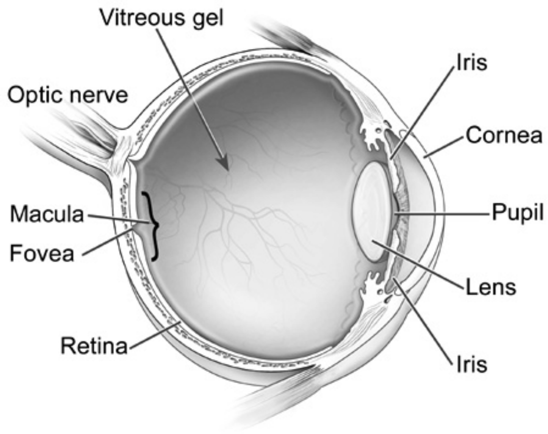

Cornea

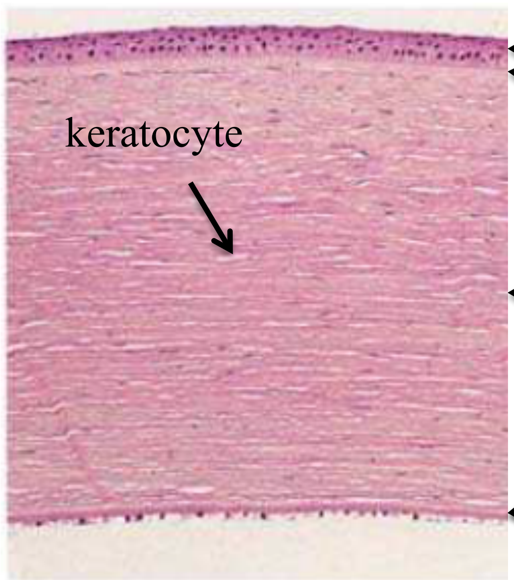

epithelium

Bowman layer → random thin — Collagen layer

stroma → regular collagen layer

Descemet layer

endothelium

collagen cross-linking (CXL) treatment

CXL treatment

riboflavin-dextran + UVA irradiation → This treatment increases corneal stiffness, slowing down the keratoconus progression

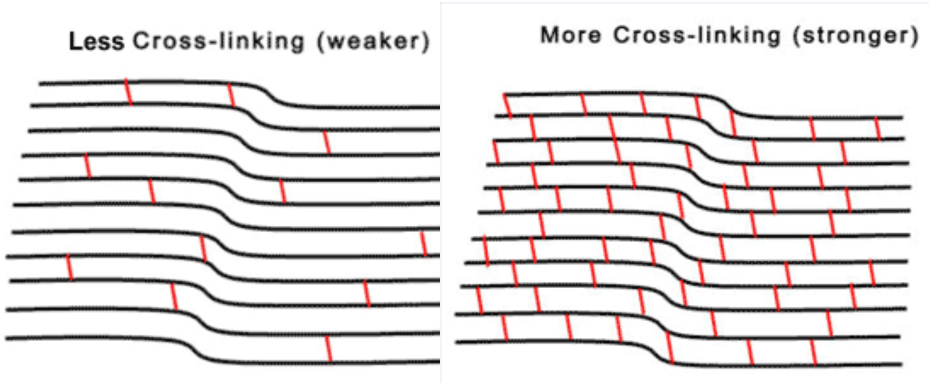

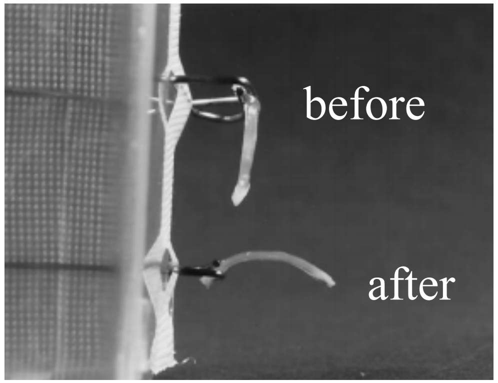

Type of Cornea	Stress at 4% (10^3 Pa)	Stress at 6% (10^3 Pa)	Stress at 8% (10^3 Pa)
Porcine			
Untreated	33.7 ± 9.3 ($E = 0.8 \times 10^6$ Pa)	57.3 ± 17.3 ($E = 1.5 \times 10^6$ Pa)	86.5 ± 29.9 ($E = 2.6 \times 10^6$ Pa)
Treated	55.8 ± 17.6 ($E = 1.4 \times 10^6$ Pa)	98.5 ± 29.7 ($E = 2.7 \times 10^6$ Pa)	151.8 ± 44.7 ($E = 5.3 \times 10^6$ Pa)
Human			
Untreated	34.3 ± 5.5 ($E = 0.8 \times 10^6$ Pa)	53.0 ± 11.5 ($E = 1.3 \times 10^6$ Pa)	79.3 ± 21.2 ($E = 2.2 \times 10^6$ Pa)
Treated	135.7 ± 61.4 ($E = 3.0 \times 10^6$ Pa)	227.3 ± 95.7 ($E = 5.9 \times 10^6$ Pa)	344.7 ± 141.9 ($E = 11.8 \times 10^6$ Pa)

Ref) Gregor Wollensak, MD, Eberhard Spoerl, PhD, Theo Seiler, MD. J Cataract Refract Surg 2003; 29:1780 –1785

Setup

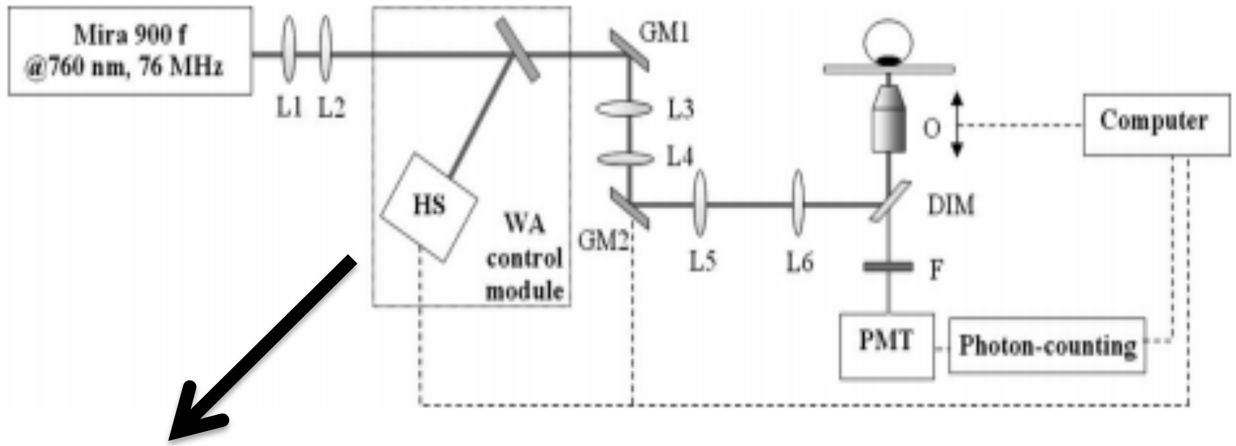

Ref) Juan M. Bueno, PhD, Emilio J. Gualda, PhD, and Pablo Artal, PhD. Cornea 2011;30:692–701

WA control module → wavefront sensor + deformable mirror

Hartmann-Shack (HS) wavefront sensor

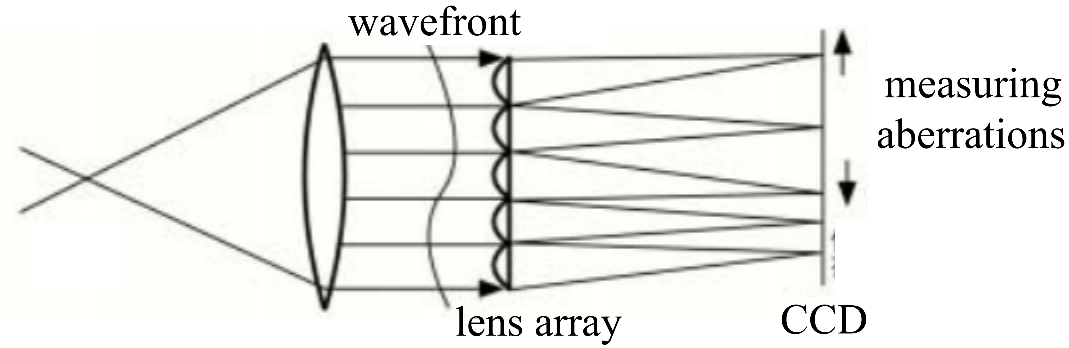

deformable mirror

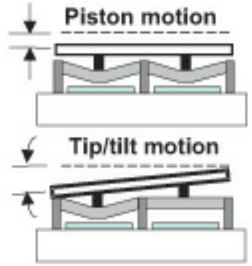

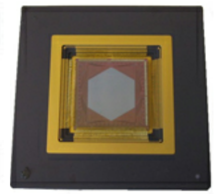

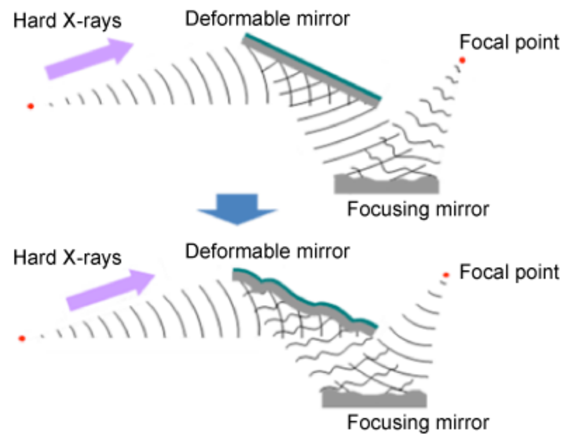

Result

SHG images of corneal stroma at different depths
captured at 0, 2, and 3 hours in an untreated porcine eye

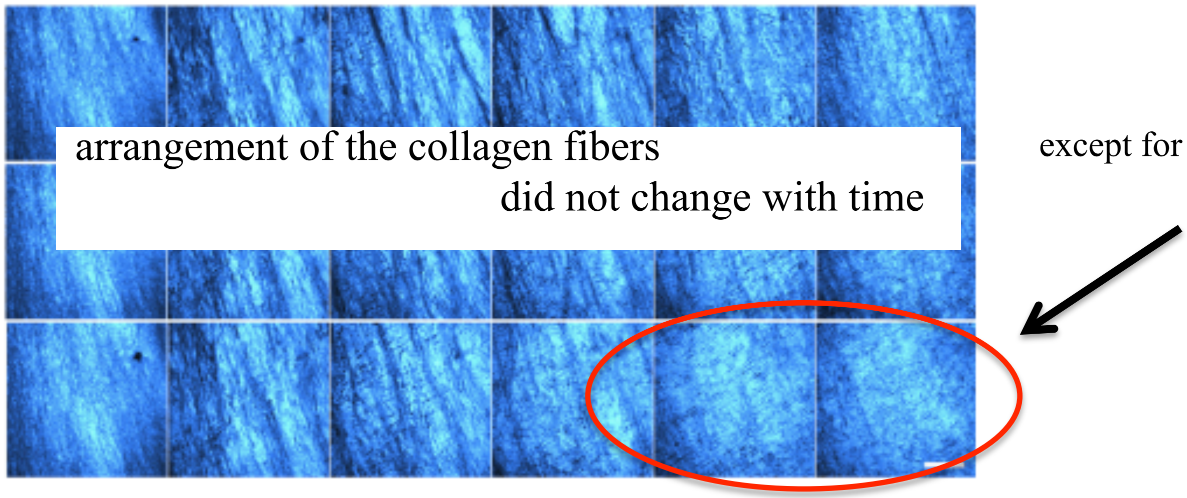

except for some minor modifications
at deeper imaged areas after 3 hours.

untreated porcine cornea (*upper panel) and*
after CXL (*lower panels)*

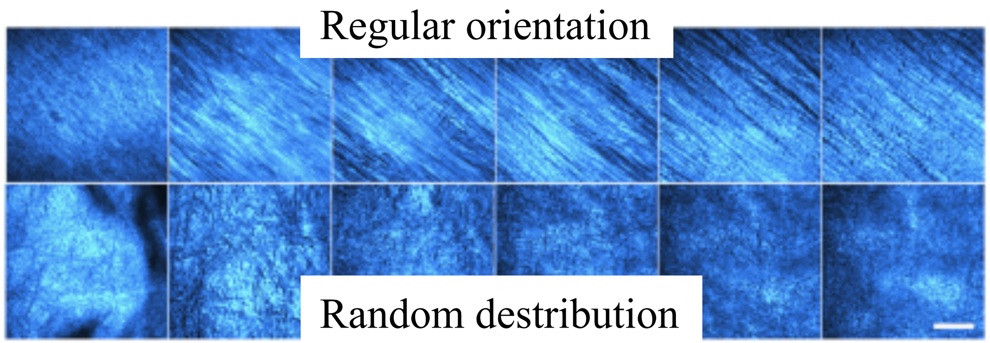

- The arrangement of the stromal collagen fibers lying mostly parallel to the corneal surface of untreated corneas is lost with the CXL

Result : Nonlinear (XZ) tomography images of porcine corneas

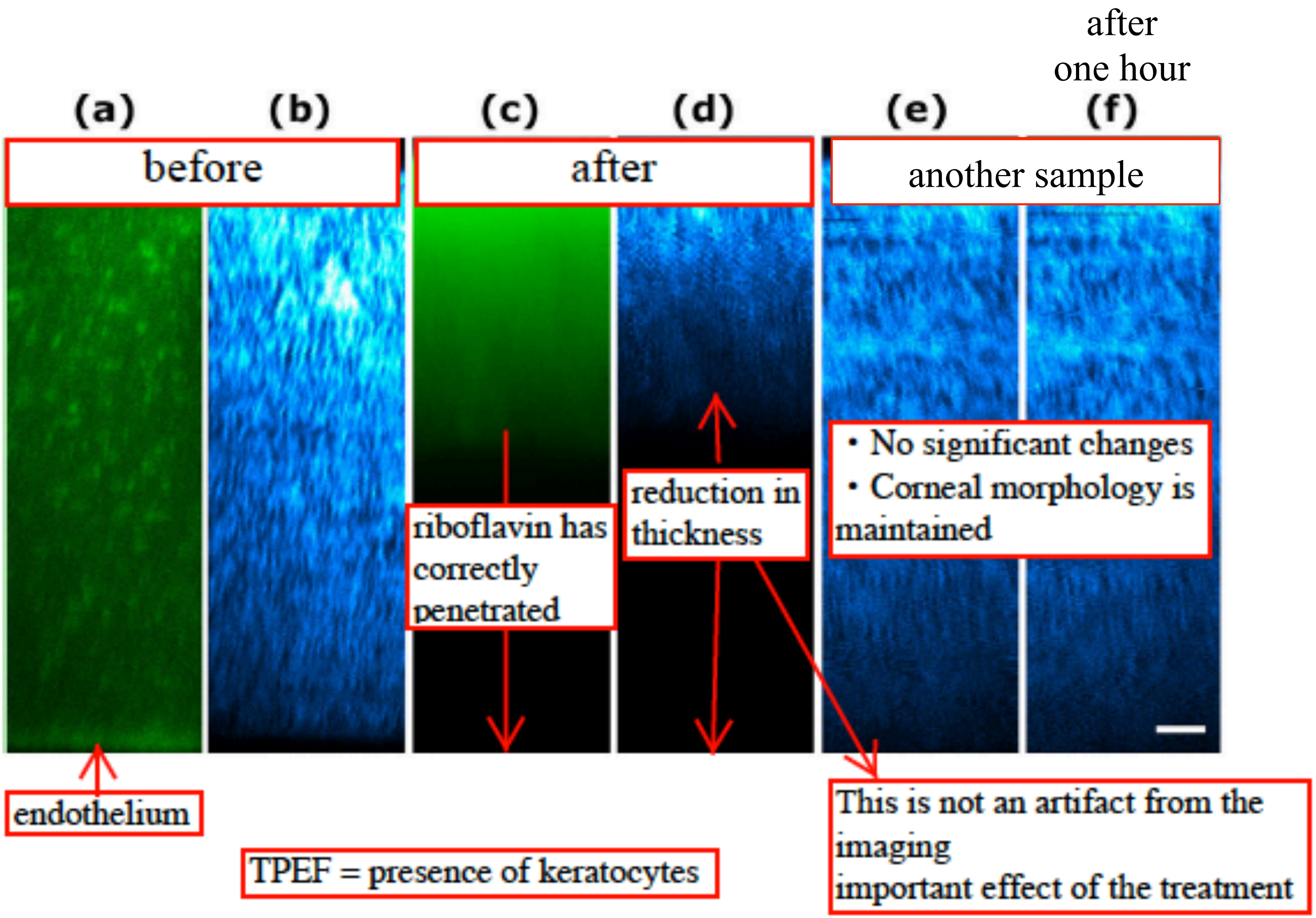

Result: Effects of riboflavin-dextran instillation in a porcine cornea

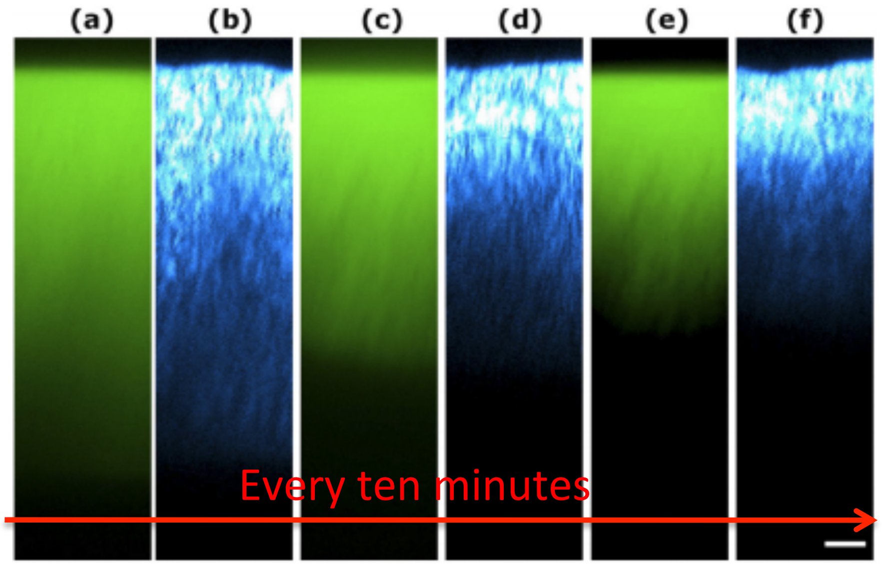

・A progressive reduction of the corneal thickness with time is observed

the dehydration effect of the riboflavin solution

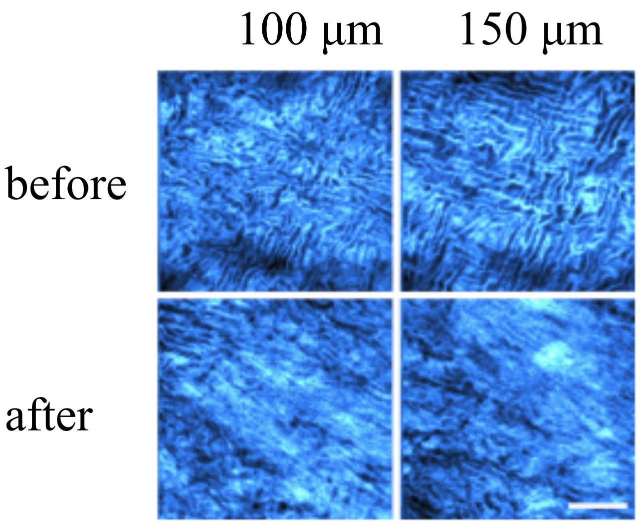

・Riboflavin is not only responsible for the reduction of corneal thickness, but also for the majority of the changes in the corneal stromal collagen arrangement after CXL.

Summary

▪A research adaptive optics nonlinear microscope has been used to visualize the structural changes in the corneal stroma after CXL treatment in bovine and porcine ex vivo eyes.

▪This author have shown structural alterations of CXL-treated corneas, which confirms the potential of this imaging modality for the analysis of the effects of this treatment.

Conclusion

- For a biomedical sample, I have to notice about
  wavelength dependence of the attenuation.

- Tooth is good sample in my study because of effect of absorption of water.

- I have to consider as what kind of tool SHG can be used.